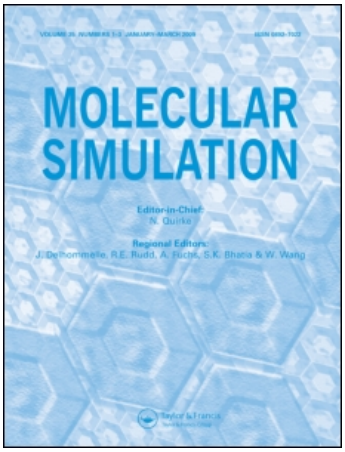

Molecular Simulation

Publication details, including instructions for authors and subscription information:
http://www.informaworld.com/smpp/title~content=t713644482

Consequences of Sequential Ca^2 Occupancy for the Structure and Dynamics of $Calbindin_{D9K}$: Computational Simulations and Comparison to Experimental Determinations in Solution

Ernest L. Mehler[a]; Joseph N. Kushick[a]; Harel Weinstein[a]

[a] Department of Physiology and Biophysics, Mount Sinai School of Medicine of the City University of New York, New York, NY

To cite this Article Mehler, Ernest L. , Kushick, Joseph N. and Weinstein, Harel(1993) 'Consequences of Sequential Ca^2 Occupancy for the Structure and Dynamics of $Calbindin_{D9K}$: Computational Simulations and Comparison to Experimental Determinations in Solution', Molecular Simulation, 10: 2, 309 — 334

To link to this Article: DOI: 10.1080/08927029308022171

URL: http://dx.doi.org/10.1080/08927029308022171

Molecular Simulation, 1993, Vol. 10(2-6), pp. 309-334
Reprints available directly from the publisher
Photocopying permitted by license only

CONSEQUENCES OF SEQUENTIAL Ca^{2+} OCCUPANCY FOR THE STRUCTURE AND DYNAMICS OF CALBINDIN$_{D9K}$: COMPUTATIONAL SIMULATIONS AND COMPARISON TO EXPERIMENTAL DETERMINATIONS IN SOLUTION

ERNEST L. MEHLER, JOSEPH N. KUSHICK and HAREL WEINSTEIN*

Department of Physiology and Biophysics, Mount Sinai School of Medicine of the City University of New York, New York, NY 10029

(Received December 1993, accepted January 1993)

Molecular dynamics (MD) simulations of the structures of calbindin$_{D9k}$ (CAB) with different occupancies of the two Ca^{2+} binding sites were carried out to gain insight into structural and energetic consequences of sequential Ca^{2+} binding. The aim of the study is to identify effects of Ca-binding site occupancy that relate to the properties and functions of Ca-binding proteins containing EF-hand motifs. Two different models of solvation were employed, one defined by a linear, distance dependent dielectric permittivity ($\varepsilon = r$) and inclusion only of the 36 crystallographically observed water molecules, and the other with the protein immersed in a 9Å shell of explicit waters and $\varepsilon = 1$. Experimental results from x-ray crystallography, and insights from NMR and from measurements of hydrogen exchange rates in these systems served as tests and guides for assessing the quality, validity and mechanistic interpretation of the results from the computational study. The results of the MD simulations agree very well with earlier experimental observations that the structure of calbindin$_{D9k}$ is rather insensitive to removal of Ca^{2+}, and indicate that this insensitivity is not dependent on the order in which the ions are removed. The calculated values of the electrostatic potentials at the Ca^{2+} binding sites are very similar, in agreement with the small differences in the measured microscopic binding constants. Details of the dynamic mechanisms of molecular flexibility revealed by the MD simulations are also in good agreement with experimental findings, including the local properties identified from comparisons of hydrogen exchange rates in various parts of the structures of sequentially occupied forms of CAB. Estimation of the changes in configurational entropy from the rms fluctuations in the structures of CAB at various levels of Ca^{2+} occupancy in the EF-hands, supports earlier suggestions relating the dynamic properties of the protein to the observed cooperativity in the binding of Ca^{2+}. The computational approaches and the results of the MD simulations are evaluated in relation to the study of effects of Ca^{2+} occupancy in calmodulin and troponin *C* where ion binding determines function and is known to trigger significant changes in structural and dynamic properties.

KEY WORDS: Molecular dynamics simulations; calcium-binding proteins; EF-hand structural motif; electrostatic potentials; configurational entropy; cooperativity in Ca^{2+} binding

1 INTRODUCTION

Computational simulations of molecular mechanisms are contributing to the rapid growth in understanding the relation between structure and function in biological

*Corresponding author

processes. By offering a representation based on energetics and dynamics, the results from computational simulations provide a link between structural and mechanistic insights into biological functions of molecules. This contribution of computational simulation to understanding molecular processes in biological systems usually depends on the availability of detailed structural information at the atomic level of resolution, appropriately related to data on the functions of the biomolecules. Such structural information is obtained from the techniques of molecular biology combined with physicochemical measurements of structure, e.g., based on x-ray crystallography and multidimensional NMR. Computational simulations often serve in the acquisition of such structural information, and are used to refine it and to interpret its relation to biological function (for some reviews see [1–10]).

Our recent work on the structural dynamics of calmodulin [11–13] provides an example of such an application of computational simulation. These calculations have revealed the role of dynamic structural changes in the function of calmodulin (CAM) – a prototypical Ca^{2+}-binding protein in the class of structures incorporating the "EF-hand" motif [14–16] that consists of a 12-residue loop flanked by two *alpha*-helices positioned at roughly right angles with respect to one another and to the binding loops. In particular, these studies identified structural elements that might be responsible for the flexibility of the tether portion of the protein and for its bending [12, 13] that produces a structural modification known to be related to the protein-binding function of CAM [17–19]. As part of an ongoing research program based on computational probing of structure and dynamics, these studies aim at a detailed understanding of the relations between structure and function in a family of calcium-binding proteins that comprises structurally related species with well differentiated functions. The diverse functions performed by the various members of this structural family include storage of Ca^{2+} (eg., $calbindin_{D9k}$; CAB), as well as Ca^{2+}-dependent binding and activation of other proteins (e.g., CAM, and troponin C; TNC); the biological functions of many other members of the EF-hand family of proteins are still unknown [20, 21]. As the functions performed by all these proteins rely on the binding of Ca^{2+}, the primary questions in the structural study of these species (for recent reviews see [16, 17, 22]) focused on the mode of binding of the ions (e.g., see [23]), the determinants of specificity and affinity for calcium (e.g., see [24–26]), and the nature of the structural response to Ca^{2+} binding that mediates the calcium-dependent function of the various proteins (e.g., see [11, 12, 18, 19, 27–33].

The available crystal structures of CAB [34], CAM [35], and TNC [36, 37] demonstrate the commonalities in the structures of their Ca^{2+}-binding regions [22, 23, 38], expressed in pairwise repeats of the element of supersecondary structure characterized early as an "EF-hand" [38, 39]. The conserved nature of the multiple Ca^{2+} binding sites in these proteins containing EF-hand motifs has been well characterized structurally from these crystal structures [16, 22, 23, 38], and genetically from the amino acid sequences [40] of the surprisingly large variety of proteins containing such sites [20]. Nevertheless, the relation between their ability to bind calcium and the various functions performed by these proteins is not well understood. In particular, the large fluctuations in cellular Ca^{2+} concentrations under physiological conditions, and the dependence of the functions of EF-hand proteins on the binding of Ca^{2+} in all or some of the binding loops, motivate the great interest in the structural and dynamic properties of these proteins at various levels of Ca^{2+}-occupancy. Recent information on the structural dynamics of such

proteins in solution [41], and about the properties of their complexes with various peptides [18, 19, 28, 30, 31, 42–44] identified subtle structural differences that may begin to explain functional characteristics. Among the properties revealed experimentally are the changes in flexibility and ion affinity upon sequential binding of Ca^{2+} [45–53]. The observed cooperativity in the binding of the Ca^{2+} ions in the pair of sites in CAB, and the structural differences between CAM in the crystal and in solution [11, 41, 54], relate the binding of Ca^{2+} to the biological function. A key element in understanding the mechanisms by which differences in structure and dynamics relate to the binding of Ca^{2+}, are the changes in the behavior of the species with sequentially occupied binding sites. Yet structural properties of proteins with various levels of occupancy of their EF-hand sites are difficult to determine, as witnessed by the fact that no crystal structures are available for more than one level of occupancy in the same protein. Nevertheless, spectroscopic data for CAB obtained in the laboratories of Forsen and Chazin, have provided most valuable insight into the nature of the changes in the properties of the protein with sequential occupation of the binding sites [46, 51–53, 55].

To gain further insight into structural and energetic consequences of sequential Ca^{2+} binding, and to enable a comparison of the effects of sequential occupancy in CAB with the properties of other EF-hand Ca-binding proteins, we carried out the molecular dynamics simulations of the structures of CAB with different occupancies of the two Ca binding sites, as presented here. The results and insights from the experimental measurements on these systems served as excellent tests and guides for assessing the quality, validity and mechanistic interpretation of the results from the present computational study of the dynamic properties of CAB at different levels of binding site occupancy. In turn, the results from the present computational simulations provide valuable insight into dynamic mechanisms of molecular flexibility that are likely to be shared by other proteins in this class, and validate some of the key inferences from the experimental work relating configurational entropy to the observed cooperativity in Ca^{2+} binding to CAB.

2 METHODS

2.1 *Starting Structures and Solvation Models*

The crystallographically determined structure of calbindin$_{D9k}$ [34] (the "x-ray structure") obtained from the Protein Data Bank [56] was used to define a set of initial coordinates for the molecular dynamics both with an explicit water bath and with model-solvent options. To construct the starting structure for the molecular dynamics simulation of the 75 residue protein with explicit bulk solvent, the 36 crystallographically determined waters were deleted and a 9Å shell of water molecules was added using the SOAK option of the InsightII software implemented on a Silicon Graphics workstation. This structure includes calbindin$_{D9k}$, the two Ca^{2+} ions bound in the loops of the EF-hands, and 1191 water molecules, yielding a system with a total of 4299 atoms. With the standard 8Å non-bonded cutoff used in the CHARMm package of simulation software [3, 57], all protein atoms are completely immersed in the 9Å water shell, and the surface effects are considered sufficiently remote to have only a negligible effect on the simulations.

Energy optimization was carried out in two steps: first the water positions were relaxed holding the protein and Ca^{2+} coordinates fixed, and subsequently

the coordinates of the whole system were relaxed. All calculations on the water immersed system were carried out with unit dielectric constant ($\varepsilon = 1$).

The resulting energy minimized structure was used to equilibrate the water bath by heating the solvent shell to 300K with a fixed protein structure, and then continuing the simulation for 30ps. An average structure was extracted from the last 16ps of this run and fully minimized. The resulting coordinate set was then used as the initial structure for the unconstrained simulations on explicitly solvated CAB.

The starting structure for the simulations with model-solvent was also obtained from the x-ray structure, but here the 36 crystallographic waters were retained to account for some of the explicit protein-water interactions. The structure was energy minimized in two steps as described above, but no subsequent solvent equilibration step was carried out. In these calculations a linear, distance dependent dielectric ($\varepsilon = r$) was used. The protocol used for the simulations is identical to that reported previously for a similar solvent model [11]: The energy minimized system is first heated to 300K in 6ps by increasing the temperature in 5° increments every 100 steps using velocity assignment, and subsequently continuing the run using temperature scaling until the structure has come to equilibrium.

In the discussion below, results from the simulations with the 9 Å shell of solvent water will be denoted by "9A", while the results from simulations which include only the crystal waters and the $\varepsilon = r$ solvent model will be referred to as "CW". The generic structures of calbindin$_{D9k}$ at various levels of Ca^{2+} occupancy will be referred to as CAB_0, CAB_1 and CAB_2 for the apo-, half- and fully occupied forms, respectively. Whenever necessary, the solvent model and order of Ca^{2+} deletion will also be denoted, e.g., CABCW signifies calbindin$_{D9k}$ from the CW simulation with CAB_2, CAB9AD1 denotes calbindin$_{D9k}$ with the 9A solvent model and Ca^{2+} deleted from the first EF-hand (EF I), etc.

2.2 *Simulations of Apo-structures and Structures Containing a Single Ca^{2+}*

The CW model was used to generate six trajectories with differing Ca^{2+} occupancies. These differ in the order in which the metal ion was removed: First, the simulation with CAB_2 was carried out, and from the final entry in the trajectory three structures were generated with one or both Ca^{2+} removed (see Table 1 for the lengths of the various MD simulations). These structures served as starting points for simulations of the singly occupied structure CAB_1 or of the apo-form CAB_0. Thus, CABCWD1, CABCWD2 and CABCWD12 represent, respectively, the protein with the Ca^{2+} removed from EF I, from EF II and from both EF hands. Other starting structures were generated by deleting Ca^{2+} from CABCWD1 and CABCWD2 to yield two additional apo-structures, CABCWD1D2 and CABCWD2D1. The coordinate set used to construct CABCWD1D2 was the snapshot of CABCWD1 at 306ps, whereas CABCWD2D1 was formed from the last coordinate set in the trajectory of CABCWD2 (see Table 1).

The 9 Å solvent model was used to carry out three simulations on the three forms CAB_2, CAB_1 with Ca^{2+} deleted from EF I, and CAB_0. Here, CAB9AD1 was generated from the coordinate set of CAB9A at 96ps and CAB9AD1D2 was constructed from CAB9AD1 using the trajectory entry at 96ps.

The same computational procedure was used for each simulation run as described above. The runs were continued until the temperature fluctuated about a well established mean with no drift over a period of 50–100ps at which point the protein

Table 1 Characteristics of simulated systems and trajectories.

System[a]	*No. of Waters*	ε	*average interval*[b]	*trajectory (ps)*[c]	*surface area (Å^2)*	*Rg (Å)*
X-ray	36				4631	11.31
CABCW	36	r	314–406	406 (313.3)	4081	10.98
CABCWD1	36	r	206–306	306 (161.5)[d]	4115	10.99
CABCWD2	36	r	106–206	206 (6.2)	4144	11.01
CABCWD12	36	r	118–206	206 (117)	4201	11.12
CABCWD1D2	36	r	508–606	606 (507.7)	4207	11.13
CABCWD2D1	36	r	106–206	206 (6.3)	4135	11.06
CAB9A	1191	1	155–200	250 (7.7)	4722	11.54
CAB9AD1	1191	1	150–200	200 (7.3)	4783	11.54
CAB9AD1D2	1191	1	150–200	200 (7.3)	4962	11.61

[a] CW = Fully loaded calbindin$_{D9K}$ and crystallographic waters; 9A = Same as CW, but with a 9Å water shell; Di = Ca^{2+} deleted from EF i; DiDj = Ca^{2+} deleted from EF i then EF j; Dij = Ca^{2+} deleted from EF i and EF j.
[b] Time interval from which average structure was computed.
[c] Length of run; in parentheses, time at which last scaling occurred.
[d] This run was continued for an additional 200ps.

was considered to have reached a local equilibrium (see Table 1 for the time at which the last velocity scaling occurred). For the structure CABCWD1, however, the simulation was continued for an additional 200ps to explore further the equilibration assumption.

3 RESULTS AND DISCUSSION

3.1 *Comparison of Structures*

The details of the trajectories computed for each of the structures are discussed in Section 3.2, below. The lengths of the runs were determined by the perceived equilibration behavior. At the end of the run for each system, average structures were calculated from approximately the last 100ps of the trajectory for the CW simulations, and the last 50ps of the 9A runs (Table 1). These were energy minimized to eliminate unphysical distances resulting from the averaging. In the case of the 9A systems the minimization consisted of two steps in which the water positions were first minimized with the protein constrained, and subsequently with the entire system relaxed.

3.1.1 *Secondary structure*

Comparison of secondary structure is most directly achieved with the help of linear distance plots (ldp) [58] (e.g., for CAM see [11]). The helix-loop-helix structure of the EF hand motif is clearly exhibited in the ldp of the x-ray structure (Figure 1A). Comparisons of Figures 1B trough 1G to the ldp in Figure 1A shows that although the overall features appear to be reasonably well conserved, the details of secondary structure identifiable in each of the ldp from the CW simulations, are quite different from those in the crystallographic structure. Most apparent is the distortion of the first helix (H1) which shows substantial loss of helical structure. The binding loop of EF I as well as H2 appear to be reasonably well conserved. EF II also

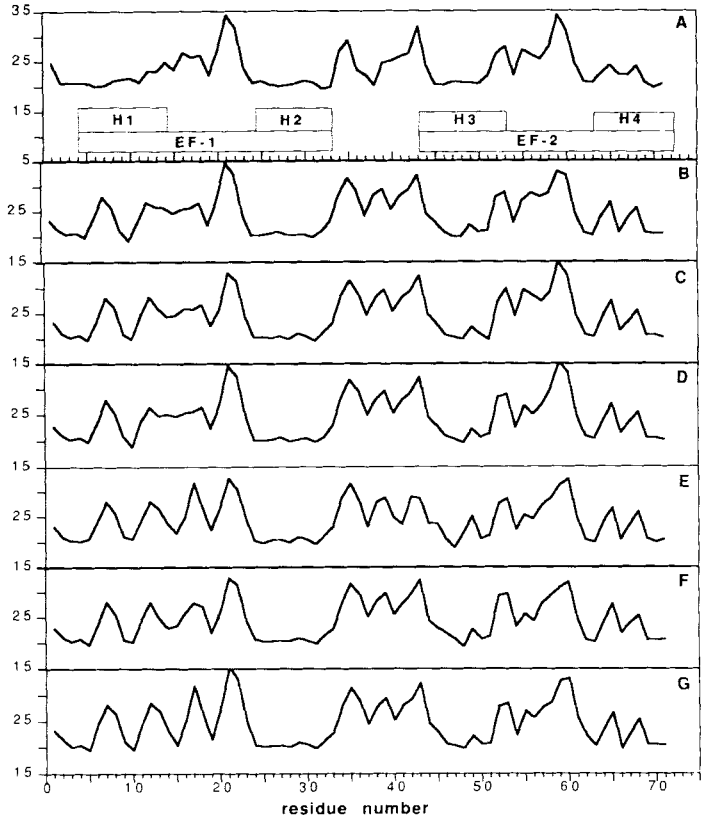

Figure 1 Linear distance plot representations of calbindin$_{D9k}$ from (A) x-ray coordinates, (B) CABCW, (C)CABCWD1, (D) CABCWD2, (E) CABCWD1D2, (F) CABCWD2D1, (G) CABCWD12. The parsing of the sequence into elements of secondary structure is identified in panel (A), together with the extent of the two EF-hands. The positions of the EF hands in the plot are defined from an rms superposition of the CAB EF-hand segments on the corresponding segments in the carboxylate domain of calmodulin.

appears to be reasonably well conserved in all the structures except CABCWD2 where H3 has become distorted.

The ldp-s for the structures resulting from the 9A simulations are given in Figure 2. Comparison of plots obtained from the various 9A structures (Figures 2B through 2D) to the ldp of the crystallographic structure (Figure 2A) shows that all the elements of secondary structure are conserved independently of Ca^{2+} occupancy. At most, minor variations are observed which have no discernible effect on the structure.

3.1.2 *RMS differences and tertiary structure*

RMS differences were calculated between the various structures and are given in Table 2 and Table 3 for the CW and 9A simulations, respectively. The rms differences between the C_α carbons of the crystallographic structure and the

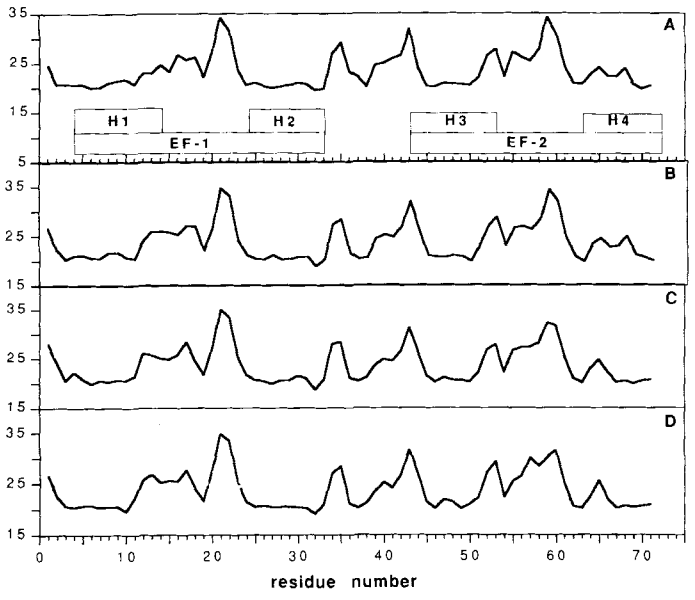

Figure 2 Linear distance plot representations of calbindin$_{D9k}$ from (A) x-ray coordinates, (B) CAB9A, (C) CAB9AD1, (D) CAB9AD1D2. See legend of Figure 1 for details.

Table 2 RMS differences from CW simulations (Å)[a].

	X-ray	CABCW	CABCWD1	CABCWD2	CABCWD12	CABCWD2D1
CABCW[b]	2.67					
EF I; EF II	2.25; 2.47					
CABCWD1	2.87	0.647				
EF I; EF II	2.47; 2.74	0.533; 0.698				
CABCWD2	2.85	0.493	0.513			
EF I; EF II	2.34; 2.65	0.258; 0.525	0.393; 0.527			
CABCWD1D2	2.98	0.782	0.887	0.888		
EF I; EF II	2.66; 2.76	0.861; 0.530	0.839; 0.645	0.835; 0.520		
CABCWD2D1	2.97	0.939	0.668	0.729	1.08	
EF I; EF II	2.42; 2.91	0.690; 0.986	0.465; 0.780	0.593; 0.684	0.841; 0.860	
CABCWD1D2	2.89	1.76	1.69	1.68	1.86	1.70
EF I; EF II	2.15; 2.85	1.10; 1.46	1.22; 1.40	1.16; 1.31	1.15; 1.45	1.16; 1.34

[a] See footnote (a), Table 1, for legend of column and row headers.
[b] rms values from superposition of Cα carbons; residues 1-75 for the whole protein, residues 1-35 for EF I and residues 45-75 for EF II.

average structures from CW simulations lie between 2.6Å and 3.0Å. The rms differences for the individual EF hands are usually smaller than the overall values, indicating that in most cases the linker between the two hands is more flexible than the two Ca^{2+}-binding motifs, a finding that is in good agreement with experimental evidence from both NMR [47, 53, 59] and crystallography (for a recent comparison see [60]). The magnitudes of the rms differences, and the relative

Table 3 RMS differences from 9A simulations (Å)[a].

	X-ray	CAB9A	CAB9AD1
CAB9A[b]	1.34		
EF I, EF II	1.07; 0.76		
CAB9AD1	1.63	1.06	
EF I; EF II	1.57; 1.17	0.82; 0.93	
CAB9AD1D2	1.39	1.14	1.05
EF I; EF II	1.30; 1.20	0.76; 1.19	0.94; 1.06

[a] See footnote (a). Table 1, for legend of column and row headers.
[b] See footnote (b), Table 2, for segment lengths included in the superpositions.

structural integrity of the EF-hands are similar to the results found earlier for CAM and TNC in simulations based on the same model to represent the solvent [11], as well as in explicit solvent environment [13]. The rms differences between the various average structures obtained from the present simulations range from about 0.5 Å to 1.8 Å and show that removal of Ca^{2+} does not have much effect on the structure of CAB. It is also evident that the CAB_0 structures resulting from the three trajectories are not very different from each other although they result from disparate trajectories started from the different orders of Ca^{2+} removal from the loops of half loaded CAB_1 structures.

Some differences emerge from a more detailed examination of the rms values in Table 2, especially in the way that the EF hands respond to removal of Ca^{2+}. However, it seems more appropriate to consider these details from the results of the explicitly solvated "9A" simulations, because the rms differences between the x-ray and the 9A structures are only 1.3 Å to 1.6 Å, much smaller than the differences obtained from the CW structures. Comparison of the rms differences calculated for the EF hands to those of the complete structures also indicates some interesting differences: For CAB9A the linker appears considerably more flexible than either EF hand, but when the Ca^{2+} has been removed, the rms difference of the corresponding EF hand is about the same as the overall value suggesting increased variability in the absence of the ion. The similarity of the structures obtained from the simulations to the x-ray structure is strikingly demonstrated in Figure 3 which shows the superposition of CAB9A, CAB9AD1, and CAB9AD1D2 on the x-ray structure. It is also of interest that the similarity between CAB9A and the x-ray structure extends beyond that observed from superposition of the main chains. Thus, the all-atom rms difference was found to be 1.9 Å, with somewhat smaller values for the EF hands.

The values of the rms differences between the three structures obtained from the simulations are given in Table 3. Only slightly over 1 Å, these small differences indicate that the 9A model predicts the overall folding of $calbindin_{D9k}$ not to be very sensitive to removal of one or both Ca^{2+} ions. This result is in complete agreement with inferences from NMR studies on CAB_0, CAB_1 and CAB_2 [50–53, 55] which indicate little change in overall structure upon removal of one or both Ca^{2+}. It is noteworthy, however, that comparing the relative magnitudes of the rms values for the EF-hands relative to the CAB9A structure, which represents the solution structure, yields a different conclusion than comparison of rms values relative to the crystallographic structure. Thus, the rms of EF I is smaller than that of EF II when the solution structure serves as standard (this is especially apparent

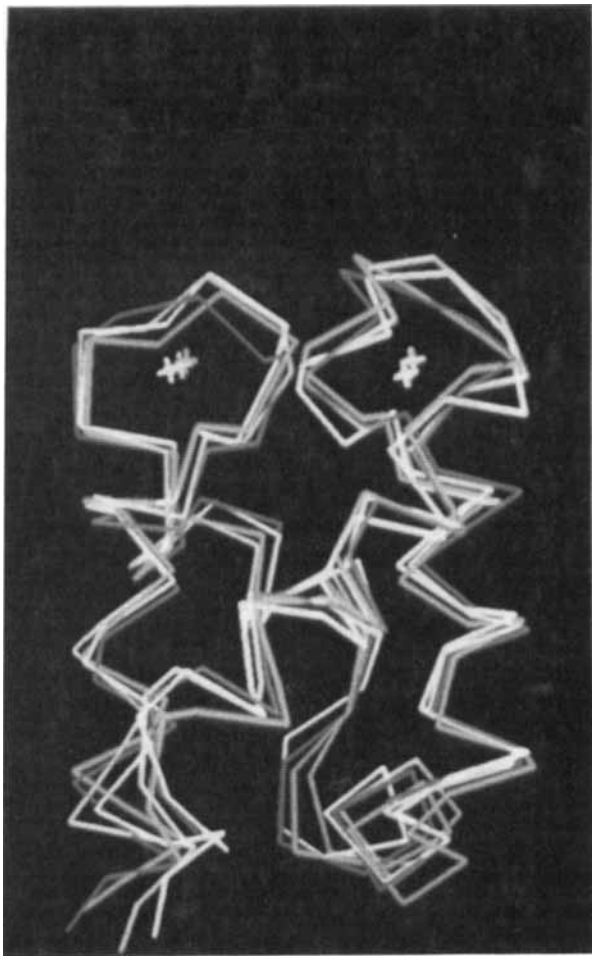

Figure 3 Superposition of Cα chains of CAB9A (*yellow*), CAB9AD1 (*magenta*) and CAB9AD1D2 (*red*) on the Cα chain of the crystallographic structure (*green*). (See Colour Plates)

for the difference between CAB9A and CAB9AD1D2). This result indicates that in going from CAB_0 to CAB_1, EF II changes more than EF I when Ca^{2+} is bound. It will be of interest to see how NMR studies resolve this question, since it implies some difference in the dynamical characteristics of the crystallographic structure compared to solution structures.

3.1.3 *Structural differences and the solvent model*

Since the CW structures, like the results from the 9A simulations, appear to be insensitive to deletion of Ca^{2+}, it can be concluded that qualitatively reliable global structural features can be determined by using a simple solvent model which includes crystal waters and a linear, distance dependent dielectric permittivity. This seems to be the case in spite of the fact that the rms differences between CW and x-ray structures is nearly 3 Å, which is also the value of the rms difference between

CABCW and CAB9A. Moreover, many, but not all, of the trends observed for the rms values of the EF hands were also correctly reproduced by the CW model. Equivalent calculations on calmodulin with and without a solvation shell lead to similar conclusions (Mehler *et al.*, to be published).

Nevertheless, simulation results obtained from simple models have to be interpreted with caution. From the calculated radii of gyration (Rg) and solvent accessible surface areas of each structure (Table 1), it appears that the CW calculations all show the typical, but artifactual, reduction of accessible surface area due to charged and polar groups folding into the protein molecule, which also leads to a small reduction in Rg. The 9Å shell of solvent clearly is sufficient to prevent this contraction.

The solvent accessible surface area in both the CW and the 9A simulations increases by about 5% in the apo-protein, suggesting that removal of both Ca^{2+} ions leads to a slightly less rigidly packed structure. Comparison of space filling models also suggests a decrease in packing as shown in Figure 4. In this particular view it appears that in the lower half of the apo-protein the molecule has opened up somewhat. Other views suggest similar changes in other parts of the molecule, but given the similarity of the structures of CAB_2 and CAB_0, these changes are fairly small.

Analyses of recent NMR and amide proton exchange experiments on sequentially occupied CAB [51, 53, 55] have come to similar conclusions: On the one hand the secondary and tertiary structures of the apo, half- and fully loaded protein are very similar, but on the other hand information about the dynamics of these structures, obtained from the proton exchange rates, suggests increased flexibility of apo-calbindin [51]. These results are in excellent agreement with the findings from the present simulations, as evidenced by the exceptionally good agreement with the details of the dynamic fluctuations and entropic contributions to the Ca^{2+} binding energies described in Section 3.4, below.

3.2 *Trajectories*

The last velocity scaling in the CABCW run occurred at 313.3ps and therefore the run was continued to 406ps. From Figure 5A it is seen, however, that the rms difference was stable from about 220ps onward. The last velocity scaling, the length of the trajectories and the time interval used for extracting an average structure are given in Table 1. The temperature drift of structures CABCWD2, CABCWD12 and CABCWD2D1 stabilized quite early in the calculation. The rms values for these three runs appeared to be stable from about 30–90ps onward (cf. Figure 5C, 5E, and 5F) and these runs were stopped at 206ps.

The trajectory of CABCWD1D2 seemed to be slow in attaining a constant average temperature, and for this reason it was continued to 600ps. Nevertheless Figure 5D shows that the rms deviations stabilized at about 240ps, and from that time onward continued simply to fluctuate about a mean value. The structure CABCWD1 behaved differently: The last velocity scaling occurred at about 160ps and the simulation was continued to 306ps. Subsequently the run was continued for another 200ps to explore both the stability of the energetics and of the rms difference from the initial structure. Although the temperature and energy remained constant, the trajectory plot in Figure 5B shows that around 330ps the structure changed to produce an increase of about 0.6Å in the rms difference. Although the change

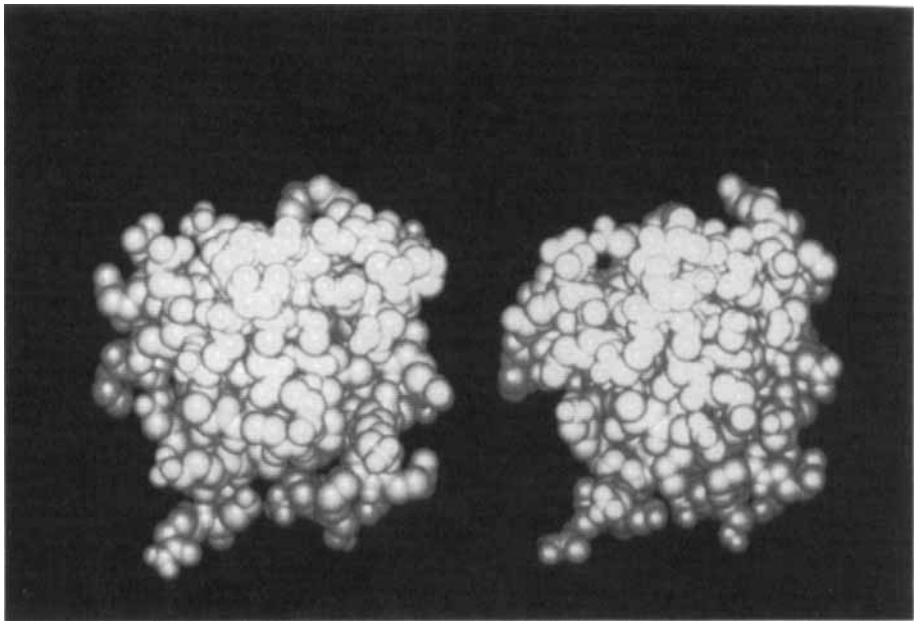

Figure 4 Space filling models of CAB9A (right) and CAB9AD1D2 (left). The Ca^{2+} are shown in *green* and the NH groups of residues 68–72 are in *blue*. (See Colour Plates)

is not large enough to alter our general conclusions that the CW runs do predict the overall structural insensitivity of CAB to Ca^{2+} removal, it is, of course not clear whether further increases would occur if the run were to be continued. It is also possible that this type of occurrence is an artifact due to the absence of explicit solvent, although the trajectories of the other long CW simulations did not exhibit such late jumps in the rms differences.

Figure 6 displays the rms differences of the 9A simulations from the x-ray structure as a function of time. The three plots clearly show that there is no substantial change in structure after the simulation of the holo-protein comes to structural equilibrium at about 150ps. The energy minimized coordinates of the snapshot at 96ps of CAB9A provided the starting structure for the removal of one Ca^{2+}. At this time the rms difference of CAB9A was around 1.1 Å, and it is clear that CAB9AD1 simply continued from this value. CAB9AD1 required about 100ps to reach its equilibrium rms value of about 1.6 Å, and then only fluctuated around that value for the last 100ps of the simulation. The starting structure for CAB9AD1D2 was taken from CAB9AD1 at 96ps where its rms value was around 1.7 Å. CAB9AD1D2 continued from this value with no significant changes over the entire 200ps of the trajectory. These results suggest that it is probably more efficient to delete the ligand from the structure of the parent obtained from an interval of the trajectory where it has attained equilibrium. The preparation of the starting structure for the simulation of CAB9AD1 from a snapshot of the parent structure taken too early in the trajectory, made it necessary to run CAB9AD1 for 100ps before it reached its final rms value. Note, however, that

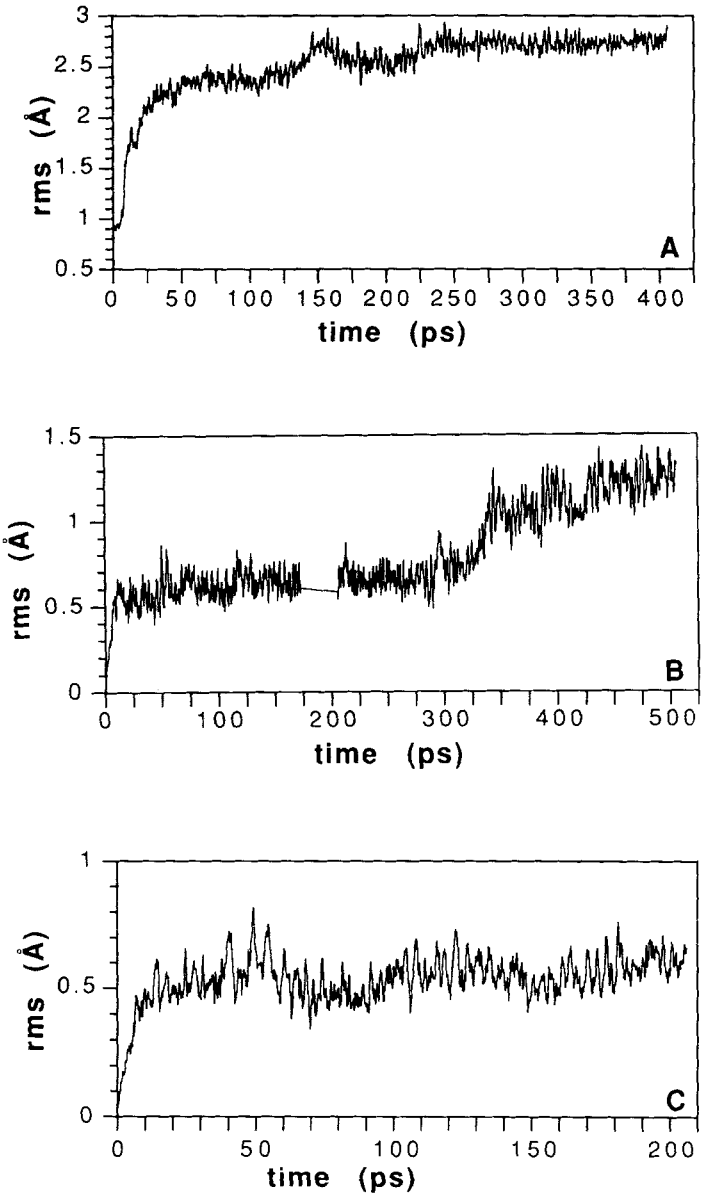

Figure 5 RMS differences (Cα) from the trajectories of the CW simulations. The difference of CABCW is between each entry in the trajectory and the x-ray structure; for the other simulations the difference is calculated from the parent structure. (A) CABCW, (B) CABCWD1, (C) CABCWD2, (D) CABCWD1D2, (E) CABCWD2D1, (F) CABCED12.

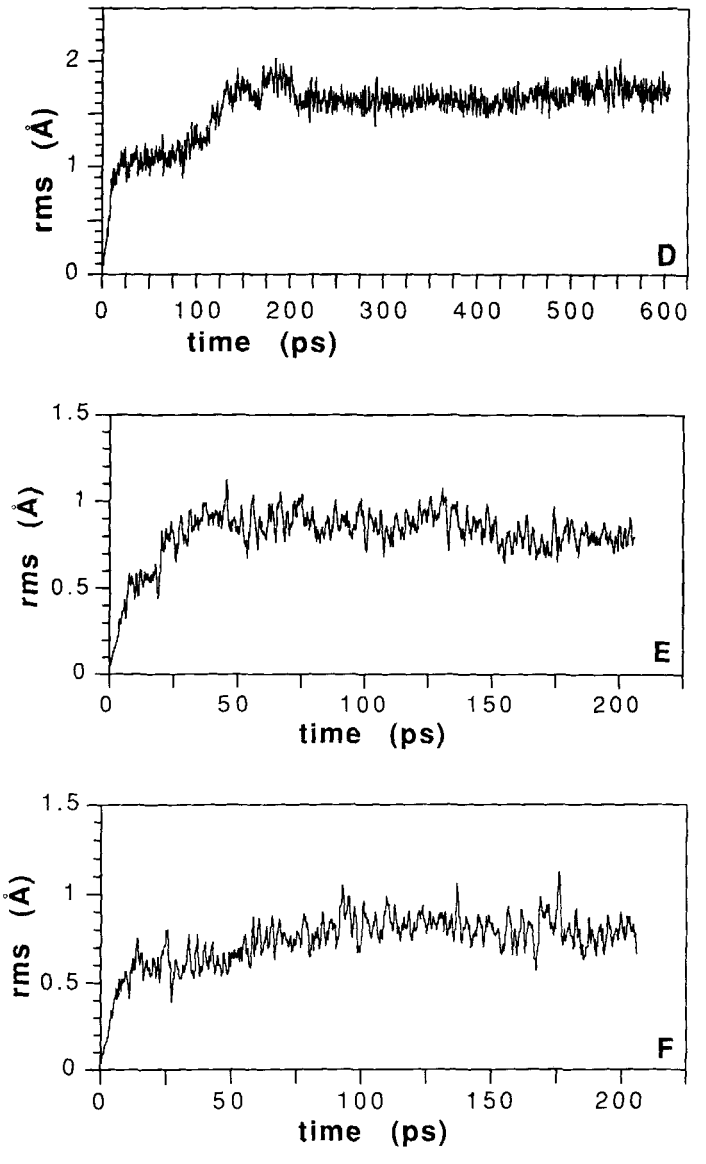

Figure 5d–f

the overall differences in structure between CAB9A, CAB9AD1 and the x-ray structure remained quite small.

3.3 *Coordination of Ca^{2+} in the Binding Loops*

Earlier calculations on CAM using the CW model for solvent effects resulted in a coordination of Ca^{2+} with too many ligands in each the four EF hands [11]. Thus,

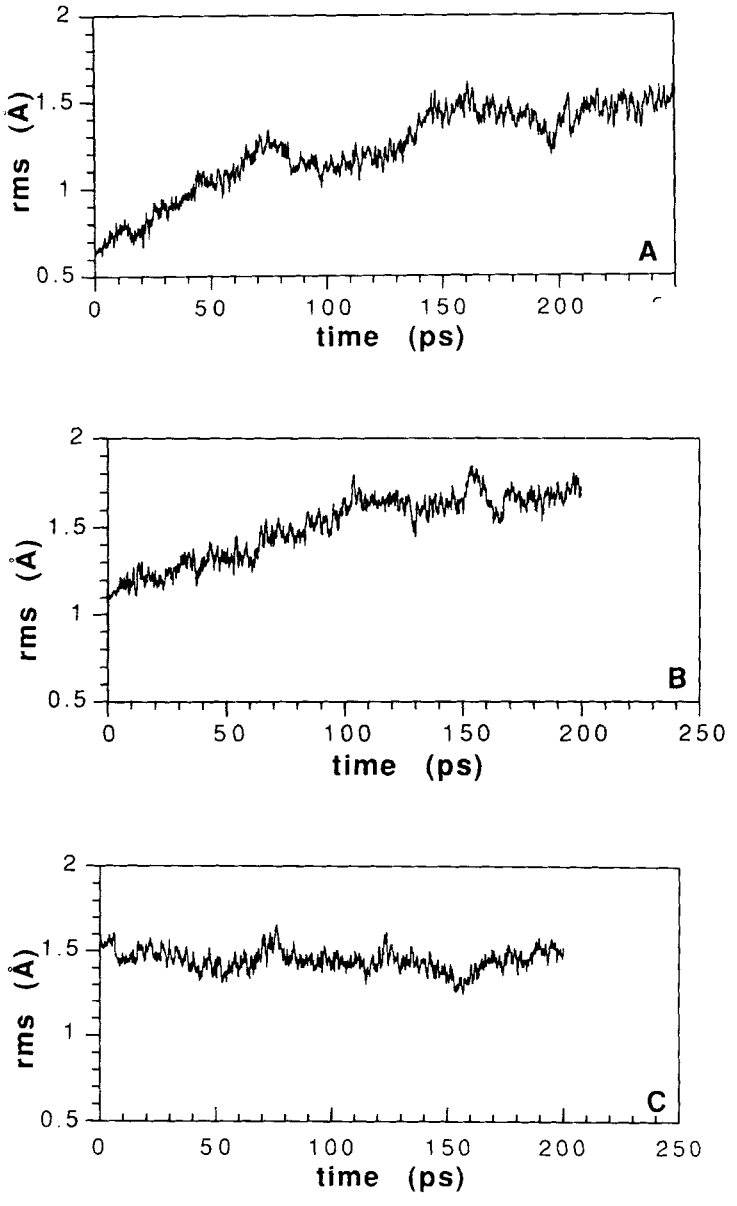

Figure 6 RMS differences (Cα) from the trajectories of the 9A simulations. The differences are between the trajectory entries and the x-ray coordinates. (A) CAB9A, (B) CAB9AD1, (C) CAB9AD1D2.

Table 4 Coordination of Ca^{2+} in various structures[a].

Residue[b]	*Atom*[b]	*X-ray*	*CAB9A*	*CAB9AD1*	*CABCW*	*CABCWD2*	*CABCWD1*
EF I							
Ala14	O	2.16	2.50		2.41	2.45	
Glu17	O	2.39	2.36		2.41	2.42	
Asp19	O	2.38	2.39		2.38	2.37	
Gln22	O	2.21	2.35		2.40	2.40	
Glu27	OE1	2.51	2.51		2.63	2.58	
Glu27	OE2	2.27	–		2.46	2.48	
Glu60	OE	–	2.54(1)		2.49(2)	2.53(2)	
H_2O	O	2.54	2.71		2.32	2.32	
EF II							
Asp54	OD1	2.38	2.48	2.58	2.56		2.62
Asp54	OD2	–	–	2.60	2.51		2.48
Asn56	OD1	2.45	2.37	2.36	2.36		2.34
Asp58	OD1	2.29	2.43	2.48	2.47		2.56
Asp58	OD2	–	–	–	–		2.49
Glu60	O	2.26	2.35	2.36	2.41		2.38
Glu65	OE1	2.29	2.59	2.70	2.51		2.49
Glu65	OE2	2.60	2.48	2.47	2.56		2.55
H_2O	O	2.25	2.60	2.60	2.33		2.35

[a] See footnote (a), Table 1, for legend of column headers.
[b] Distance in Å between Ca^{2+} and listed atom from residue given in first column.

instead of a coordination of seven observed in the crystal structure, the simulations produced coordination numbers of 8 or 9. The crystal structure of CAB also gives a coordination of seven for the Ca^{2+}, but molecular dynamics simulations by Ahlstrom *et al.* [61] resulted in coordination numbers of 8 for both EF hands. The differences between their ligation and that of the x-ray structure was in the involvement of both carboxyl oxygens of Glu60 from loop II in the coordination of the Ca^{2+} of EF I, and the loss of the carbonyl oxygen of Ala14 to the ligation shell. In the second EF hand the increase in coordination number was primarily due to the change of Asp54 ligation from monodentate to bidentate.

The 9A simulation of CAB_2 produced a coordination of 7 for both EF hands, although the ligands of EF I are not exactly identical to those observed in the x-ray structure. The coordination shell obtained from the simulations and the x-ray structure are given in Table 4. Like Ahlstrom *et al.* [61], we observed the involvement of the carboxylate of Glu60 in the ligation of the Ca^{2+} in EF I, but here it was only monodentated. In addition, Glu27 which is bidentated in the crystal structure, becomes a monodentated ligand in the structure from the present simulation. The coordination of EF II obtained from the simulation involves the same groups and atoms as the x-ray structure, but the distances between the ligating atoms and Ca^{2+} have changed. The distance of the water ligand is substantially larger in the simulation than in the x-ray structure. As described in the METHODS section, all the crystal waters were deleted from the structure before the 9Å shell of discrete waters was added. At the start of the simulations, therefore, no waters were coordinated to the Ca^{2+}, and, in fact, a snapshot taken at around 100ps still had no water in the ligation shell of either EF hand. Because the structure resulting from the simulation incorporates a water ligand in the correct geometry

with respect to the crystal structure, it can be concluded that the force field used for the calculations (PARM19 and the Ca^{2+} parameters described earlier [62]) is sufficiently reliable to reproduce the observed Ca^{2+} ligation – including a water being recruited as ligand from the surrounding bulk solvent – when the solvent is represented by the inclusion of explicit water molecules.

As observed earlier [11], CW simulations yield increased coordination of the Ca^{2+}. In EF I, coordination has increased from 7 to 8 due to the involvement of the Glu60 coordination side chain, whereas in EF II both Asp54 and Asp58 change from monodentated to bidentated ligands, increasing the coordination to 9.

The involvement of Glu60 in the coordination of EF I, not observed in the crystal structure, has now been observed in all reported simulations of CAB. However, the results presented here, which conserve the total coordination number of EF I, suggest that the binding loop may be a more dynamic structure than suggested from the x-ray structure. This could be due to the fact that this region experiences considerable interaction with the surrounding solvent which is probably greater for the protein in solution than in the crystalline state. Another source of evidence that the coordinates of Glu60 may indeed be different in solution compared to the crystal comes from electrostatic considerations. Recent mutation studies, aimed at determining the effect of charge annihilation on the binding constant of Ca^{2+}, yielded pK shifts over several orders of magnitude [45, 46]. Attempts to calculate the observed pK shifts using various macroscopic approaches and the x-ray coordinates of calbindin$_{D9k}$ [49, 63], were, with one exception, quite successful regardless of which method was used. The exception was the mutation "E60Q" of Glu60 to Gln60, where the calculations strongly overestimated the measured pK shifts [49], thus supporting the proposal that the coordinates of Glu60 in solution are different from those in the crystal, as found here and in previous studies [61, 62].

3.4 *Ca^{2+}-binding and the Flexibility of Calbindin$_{D9k}$*

3.4.1 *Atomic fluctuations*

The atomic B factors obtained from the x-ray study of calbindin$_{D9k}$ (Figure 7A) show that the residues belonging to the central portion of each EF hand are much more rigid than the linker region and the two termini of the protein (cf., results from NMR [47, 50, 52, 53, 59] and from crystallography [60]). From the evaluation of $B = \langle r^2 \rangle 8\pi^2/3$ it is possible to relate the atomic fluctuations obtained from the simulation trajectories to the observed B factors. As shown by aggregate values in Table 5, the rigidity differs in the two halves of the molecule; results for the x-ray structure indicate that the N-terminus half is somewhat more rigid than the C-terminus. The simulation of CAB9A yields somewhat smaller values for the fluctuations (as observed from the overall pattern in Figure 7), but the relative rigidity of the two halves is the same as in the crystal structure. Removal of Ca^{2+} from EF I increases somewhat the fluctuations, and now the average value for the N-terminal half is larger than for the C-terminal half where Ca^{2+} is still bound (Table 5).

Figure 7C shows that after removal of Ca^{2+} from EF I there are a few residues with fluctuations substantially larger than the mean, and the minimum observed for CAB_2 in the region between residues 20 and 30 (Figure 7A), has all but disappeared. However, the decrease in fluctuations of the residues in the central

portion of EF II is still clearly present. Thus the general characteristics of the fluctuations of CAB_2 are maintained in CAB_1. Due to the increase in the atomic fluctuations when both Ca^{2+} are removed, the B values are substantially larger, although the increase is by no means uniform. Somewhat more than half of the residues have values of less than 50 Å^2, and thus are in the same range as the fluctuations found in CAB_1 and CAB_2. It is also seen that the regions of very large fluctuation are clustered, involving several residues at the N-terminus, and groups of residues in and around the central regions of the EF hands, i.e., just those segments that were most rigid when Ca^{2+} was bound. In view of these large values it is perhaps surprising that the tertiary structure of this protein remains so close to CAB_2 (see Section 1). Examination of Figure 7D shows that there are well defined regions where the rms values are small, and these are distributed throughout the structure. This becomes clear from the rms fluctuations of the C_α carbons (not shown): There are four distinct regions where two or more residues have B values less than 20 (rms < 0.87 Å), and these are presumably sufficient to preserve the structure. Nevertheless in view of the relative insensitivity of the average structure of CAB to removal of Ca^{2+}, as described in Section 1 above and shown by NMR studies [50–53], the very large increase in the average value of the rms fluctuations when both Ca^{2+} are removed was unexpected.

3.4.2 *Details of CAB dynamics: Observed and simulated consequences of Ca^{2+} binding*

The RMS fluctuations (Table 5, Figure 7) suggest that the flexibility of CAB depends on Ca^{2+} binding, and it increases in the order $CAB_0 > CAB_1 \geqslant CAB_2$. This is the same order as concluded from recent NMR and proton exchange studies by Akke *et al.* [51]. Both changes in amide proton exchange rates and in the measured chemical shifts were interpreted to indicate a decrease in flexibility of the protein on binding metal ion; the decrease is largest for binding the first ion.

This agreement between the results of the present study and the experimental findings extends to the details of the local dynamics in CAB. Thus, residues 68 and 70–72 were found to have a slower exchange rate in CAB_0 than in either CAB_1 or CAB_2 (see Figure 5 in Akke *et al.* [51]), contrasting with the overall higher exchange rates in the apo-structure. These findings coincide with inferences from the present molecular dynamics simulations. Thus, as seen in Figure 4, the marking of the NH groups of residues 68–72 reveals that Val70, Lys71 and Lys72 are considerably more exposed in CAB9A than in CAB9AD1D2, while Leu69, which has a very slow exchange rate [51], is not seen in either molecule because it is buried in both structures. In contrast, Val68 appears to be exposed, about equally in both structures shown in Figure 4. The total solvent accessible surface area calculated for the peptide group of Val68 with a 1 Å probe is about 10 times larger in CAB9A than in CAB9AD1D2, suggesting that the amide group proton is accessible for exchange.

Another detailed experimental observation made by Akke *et al.* [51] concerns the ring flip rate of Phe10, which is found to be consistent with an increased flexibility in CAB_0 relative to the CAB_1 and CAB_2 structures. NOE distances between the NH group of Leu23 and Cε and Cζ of Phe10 suggested structural similarity between CAB_1 and CAB_2, but greater flexibility in the apo-form. In agreement with these findings, the calculated distance from the amide proton to (the closest of) the Cε or Cζ, lies between 3.9 Å to 4.2 Å for the holo-structure CAB9A, the singly

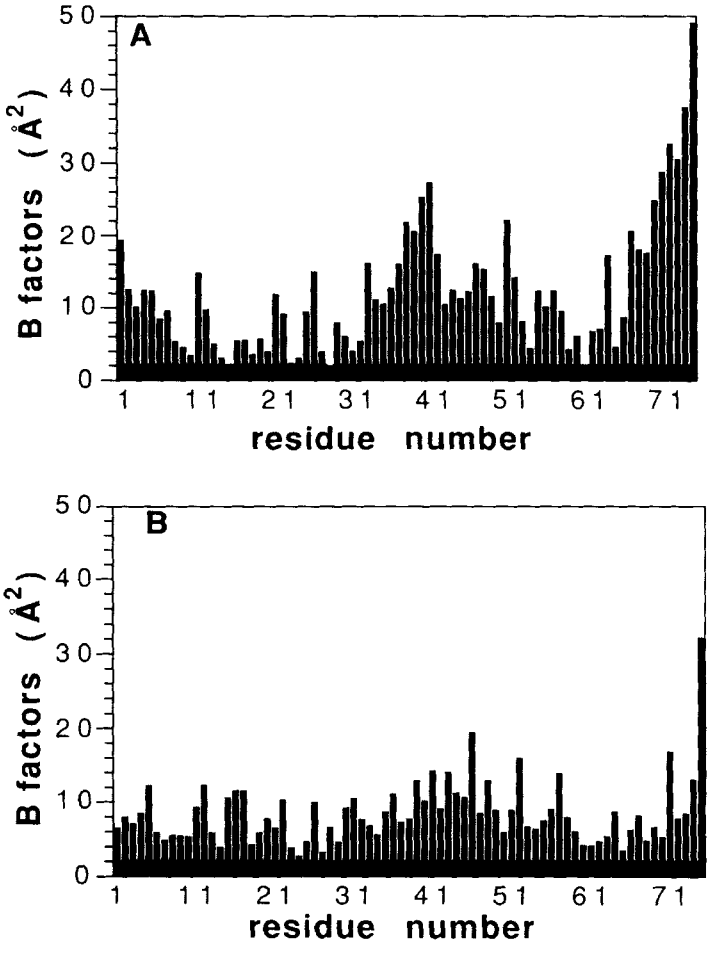

Figure 7 Atomic B factors of each residue for the x-ray and 9A simulation structures. (A) x-ray structure, (B) CAB9A, (C) CAB9AD1, (D) CAB9AD1D2.

occupied CAB9AD1, and the crystallographic structure. But this distance increases to 5.3 Å in the apo-structure CAB9AD1D2, in good agreement with the observed trend of the NOE [51]. In the crystal structure the ring of Phe10 packs underneath and between the Ca^{2+} binding loops. This is seen in Figure 8 which also shows that the phenyl rings of Phe10 in the CAB9A and CAB9AD1 structures lie close together with that in the x-ray structure, and pack tightly between the loops. In contrast, the ring of Phe10 in CAB9AD1D2 has moved towards the termini of the loops, into a less crowded region of the protein. The increase in space available to the ring is also indicated by an increase from 40 $Å^2$ to 75 $Å^2$ in the surface area of the side chain accessible to a 0.53 Å probe.

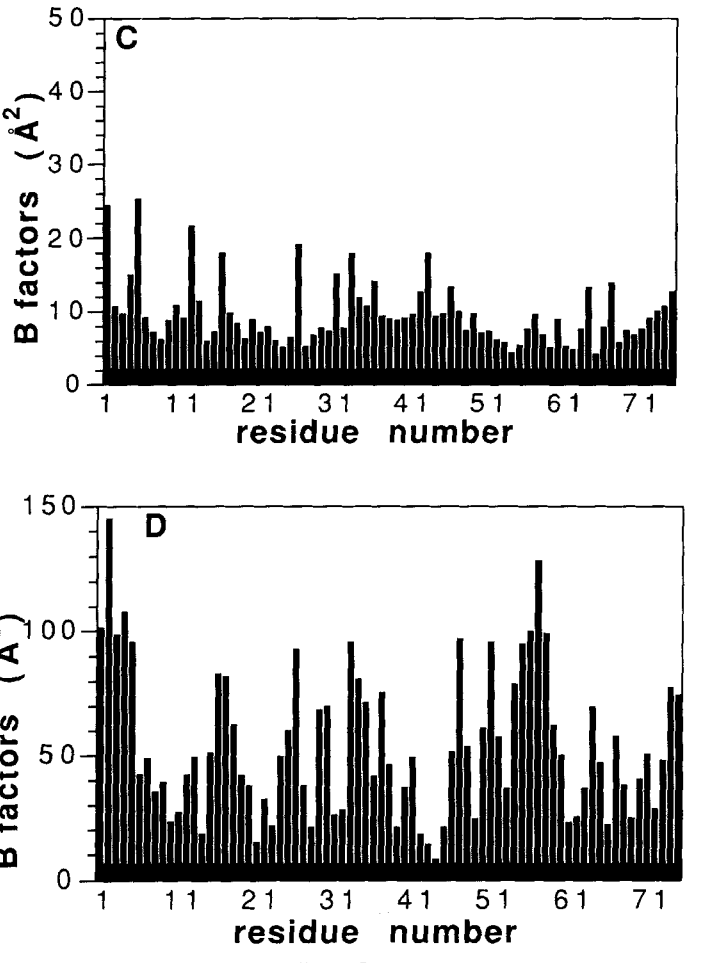

Figure 7c–d

3.4.3 *Electrostatic potentials*

To evaluate the relative electrostatic attraction of Ca^{2+} ions to the two binding sites, the electrostatic potential (ESP) values at the calcium binding sites, due separately to the liganding groups as well as to the complete protein system have been calculated for the various structures using the method of Mehler and Eichele [64]. (Note that the groups are defined by the CHARMm topology file and all atoms of a group are included in the calculation. EF I of the x-ray structure does not include the carboxylate group of Glu60.) The results are given in Table 6 for ionic strengths of 0.0 and 0.15. The protein is found to have a large effect on the potentials generated by the liganding groups at both values of the ionic strength. In all the structures, the ligands alone generate potentials which are substantially lower at site II than at site I. In the x-ray structure the effect of the rest of the protein is to reverse the order of the potentials, but the calculated difference is substantially larger than the observed cooperativity. In the structures obtained from the simulations, the charge distribution of the entire protein generates ESP values that are essentially identical at the two sites.

Table 5 RMS fluctuations from x-ray structure and 9A simulations (Å).

System[a]	*Residues* 1-75	1-37	38-75
X-ray	0.773	0.624	0.866
CAB9A	0.575	0.536	0.612
CAB9AD1	0.611	0.655	0.574
CAB9AD1D2	1.443	1.478	1.407

[a] See footnote (a), Table 1, for legend of row headers.

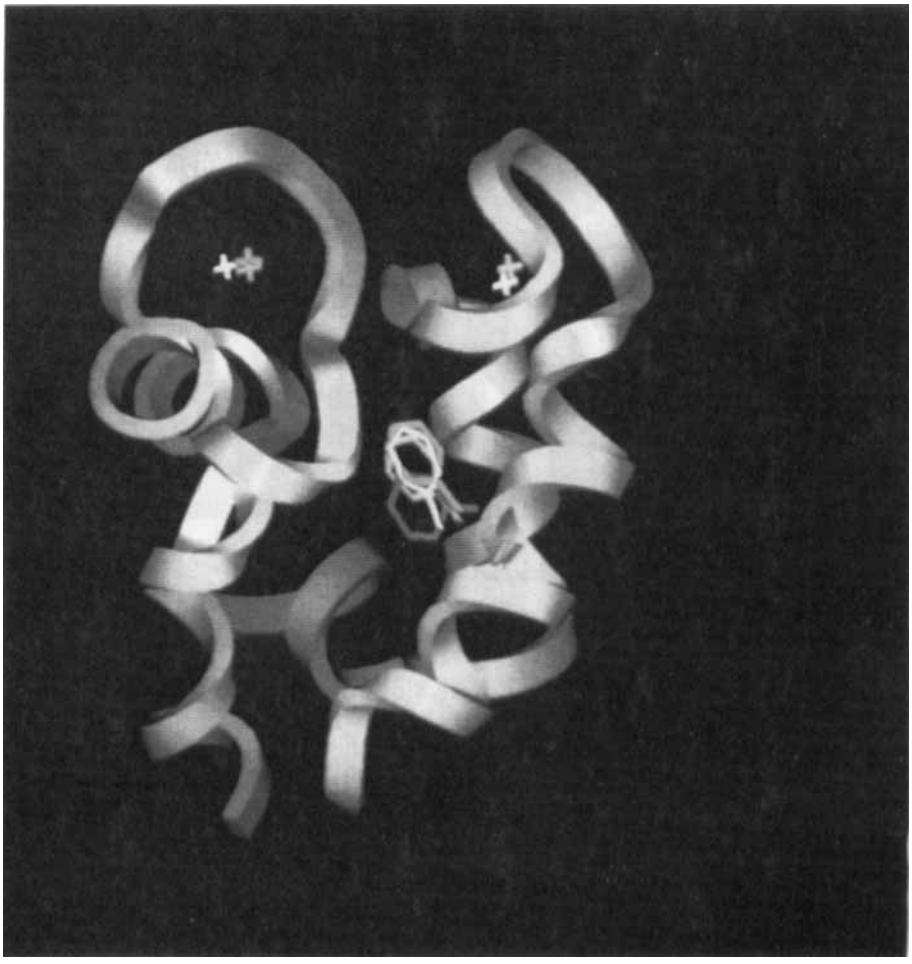

Figure 8 Disposition of the side chain of Phe10 in the x-ray and 9A simulations. The backbone ribbon is drawn from the coordinates of CAB9A. Color code of Phe10 is the same as in Figure 3: CAB9A (holo-structure; *yellow*), CAB9AD1 (half-occupied structure; *magenta*) and CAB9AD1D2 (apo-structure; *red*). (see colour plates)

Table 6 Electrostatic potential at Ca^{2+} sites in various structures (kcal/mol).

	EF I		*EF II*	
	Ionic strength		*Ionic strength*	
	0.0	*0.15*	*0.0*	*0.15*
X-ray[a]				
liganding groups	−29.5	−22.8	−33.1	−23.4
all groups	−32.2	−23.5	−29.3	−20.3
9 A				
liganding groups	−38.9	−29.6	−42.8	−31.8
all groups	−36.0	−27.2	−36.2	−27.2
9 AD1				
liganding groups			−43.6	−32.4
all groups			−37.7	−28.1
CW				
liganding groups	−42.6	−32.7	−46.6	−34.9
all groups	−43.0	−32.1	−43.6	−32.1
CWD2				
liganding groups	−42.3	−32.4		
all groups	−43.6	−32.1		
CWD1				
liganding groups			−47.9	−35.9
all groups			−46.2	−33.8

[a] See footnote (a), Table 1, for legend to row headers.

The potential at site II in CAB9AD1 is 1.5 Kcal/mol lower than in CAB9A, and the results from CABCWD1 and CABCWD2 suggest that the potential at site I in CAB9AD2 would be somewhat less affected than at site II. It seems reasonable therefore to assume that the potentials at the two sites of the apo-protein are also about the same, which agrees with the experimentally determined relation stating that $1 < K\ II/K\ I < 3$, where K I and K II are the microscopic binding constants at sites II and I, respectively (see recent discussion [51]).

3.4.4 *Configurational entropy and the cooperativity of Ca^{2+} binding*

The cooperativity in binding the second Ca^{2+} to the CAB_I form containing one calcium ion in any one of the binding loops, $\Delta\Delta G$, has been attributed by Akke *et al.* [51] to the entropic contribution to ΔG resulting from the reduction in flexibility with the binding of the first Ca^{2+}, i.e.,

$$-T\Delta S = \sim\Delta\Delta G = \Delta G_{I,II} - \Delta G_I = \Delta G_{II,I} - \Delta G_{II}$$

where $\Delta G_{I,II}$, ΔG_I, $\Delta G_{II,I}$ and ΔG_{II} are the free energy changes upon binding Ca^{2+} in the order indicated (see Figure 1 in [51]).

As the results from the present dynamics simulation agree with the flexibility changes observed by Akke *et al.* as described above, it is tempting to estimate from these data the magnitude of the entropic contribution to the calculated fluctuations of the various species. Karplus and Kushick [65] have proposed a method for calculating configurational entropies based on the matrix of the covariances of fluctuations of internal atomic coordinates. The diagonal matrix elements are mean square fluctuations (which increase the configurational entropy), while the off

diagonal elements measure the correlations between the fluctuations (which decrease the entropy). Condensing the matrix to just the value of the rms fluctuation, yields a first approximation of the configurational entropy that can be calculated directly from the values in Table 5. Making use of this approximation, the entropy difference between states A and B of the protein becomes

$$\Delta S(A \rightarrow B) = R\ln(rms)_B/(rms)_A$$

For the transition from the apo-protein to the singly occupied form, the entropic contribution to ΔG will be

$$\Delta G(CAB_0 \rightarrow CAB_1) \sim -RT\ln[rms(CAB9AD1)/rms(CAB9AD1D2)] = 1.2\,\text{Kcal/mol}$$

(based on rms results from Table 5). Similarly, the transition from the singly- to the doubly occupied form will contribute

$$\Delta G(CAB_1 \rightarrow CAB_2) \sim -RT\ln[rms(CAB9A)/rms(CAB9AD1)]) = 0.1\,\text{Kcal/mol}$$

The calculated values reflect the observation that the loss of flexibility of the singly occupied form relative to the apo form of the protein (i.e., for $CAB_0 \rightarrow CAB_1$), is much greater than upon the binding of the second Ca^{2+} (i.e., for $CAB_1 \rightarrow CAB_2$). For this reason, the entropic contribution to the cooperativity $\Delta\Delta G$ is negative in sign. The calculated value of $\Delta\Delta G \sim -1.1$ kcal/mol compares quite favorably with the experimental estimates which lie between -1.0 and -1.8 Kcal/mol (cf., Table IV in [66]). This result lends further support to the proposal that the molecular basis of cooperativity is the nature of the differential changes in protein dynamics produced in $calbindin_{D9k}$ by the binding of the first Ca^{2+} compared to the second Ca^{2+}.

4 CONCLUDING REMARKS

The results of the simulations presented here agree with earlier experimental observations that the structure of $calbindin_{D9k}$ is rather insensitive to removal of Ca^{2+}. Moreover, it appears that this is the case regardless of the order in which the ions are removed. The latter conclusion is based on the results obtained from the simulations using a model representation of the solvent defined by a linear, distance dependent dielectric permittivity and inclusion only of the 36 crystallographically observed water molecules. However, since the results also match the conclusions from calculations of the protein immersed in a 9Å shell of explicit waters, it is attractive to propose that such global structural changes (or their absence) can be evaluated qualitatively with a relatively economical representation of some of the effects of the solvent.

However, the results presented here indicate that other aspects of the simulations with the more approximate solvent model were subject to some of the same pitfalls associated with vacuum calculations. These include artifactual changes in solvent accessibility of surface residues, deterioration of secondary structural elements, and both loss of main chain hydrogen bonding [11], and appearance of artifactual H-bonds [67]. As a result, the patterns of the atomic rms fluctuations were affected. Consequently, inferences from simulations that depend on evaluation of properties that were shown to be affected by the solvent model must be approached with caution and tested with the more complete representation of the solvent environment.

It is more difficult to decide whether model solvation directly affected the results for the coordination of the Ca^{2+} ions, as it is possible that differences in the crystal and solvent environment may have an effect on the coordination. Although much closer to the coordination structure observed in the crystal, the coordination obtained from the simulations for the water-immersed protein still exhibits important differences in comparison to the observed x-ray structure.

The agreement of local structural details obtained from the simulations with results from experiments aimed at assessing the dynamic aspects of the effects of Ca^{2+} binding, are especially encouraging. These details, obtained for the explicitly solvated structures, matched the results from experiment both when they represented the general trend of the apo-structure towards increased flexibility, and when they mirrored the departure from this general trend in the properties of locally confined residues. This success lends credibility to the evaluation, albeit approximate, of the cooperativity from the entropic contribution to the change in free energy of binding Ca^{2+} to CAB, based on the dynamic fluctuations of the protein. According to the suggestion of Akke *et al.* [51], this constitutes a key component in the observed cooperativity in Ca^{2+} binding to this prototypical EF-hand protein. As these details are essential for understanding the mechanisms involving Ca^{2+} in biological processes, it becomes attractive to consider similar computational simulations of sequential Ca^{2+} occupancy in proteins such as CAM and TNC where ion binding is likely to trigger more significant changes in the structures of the proteins and in their dynamic properties.

Acknowledgements

The work was supported in part by NIH grant GM-41373, a Research Scientist Award DA-00060 from the National Institute on Drug Abuse (to HW), and a Swiss National Science Foundation Grant 31-8840.86 (to ELM). Some of the computations were performed on the supercomputer systems at the Pittsburgh Supercomputer Center (sponsored by the National Science Foundation), and the Cornell National Supercomputer Facility (sponsored by the National Science Foundation and IBM) - as well as at the Advanced Scientific Computing Laboratory at the Frederick Cancer Research Facility of the National Cancer Institute (Laboratory for Mathematical Biology) and at the University Computer Center of the City University of New York.

References

[1] J.A. McCammon and S.C. Harvey, *Dynamics of Proteins and Nucleic Acids*; Cambridge University Press, New York (1987).
[2] J.A. McCammon, "Computer-aided molecular design", *Science*, **238**, 486-491 (1987).
[3] C.L. Brooks, M. Karplus and B.M. Pettitt, *Proteins: A Theoretical Perspective of Dynamics, Structure, and their Thermodynamics*; John Wiley & Sons, New York (1988).
[4] W.F. van Gunsteren, "The role of computer simulation techniques in protein engineering", *Prot. Engng.*, **1**, 5-13 (1988).
[5] W.F. van Gunsteren and P.K. Weiner (Eds.), *Computer Simulation of Biomolecular Systems*; ESCOM, Leiden, The Netherlands (1989).
[6] B. Jonsson (Eds.), *Structure and dynamics in biological systems*; Cambridge University Press, Cambridge, New York (1989).
[7] M. Karplus and G.A. Petsko, "Molecular dynamics simulations in biology", *Nature*, **347**, 631-639 (1990).

[8] H. Weinstein and R. Osman, "Molecular biophysics of specificity and function in enzymes, receptors and calcium binding proteins", in *Theoretical Biochemistry and Molecular Biophysics: A Comprehensive Survey*, (D.L. Beveridge and R. Lavery, Eds.) Adenine Press, NY, 275–289 (1989).

[9] W.F. van Gunsteren, R.M. Brunne, A.E. Mark and S.P. van Helden, "Computer simulation of biomolecules: Comparison with experimental data", in *Molecular Aspects of Biotechnology: Computational Models and Theories*, (J. Bertran, Eds.) Kluwer Academic Publishers, Dordrecht, The Netherlands, 105–122 (1992).

[10] H. Weinstein, "Computational simulations of molecular structure, dynamics and signal transduction in biological systems: Mechanistic implications for ecological physical chemistry", in *Ecological Physical Chemistry*, (L. Bonati, U. Cosentino, M. Lasagni, G. Moro, D. Pitea and A. Schiraldi, Eds.) Elsevier, Amsterdam, 1–16 (1992).

[11] E.L. Mehler, J.L. Pascual-Ahuir and H. Weinstein, "Structural dynamics of calmodulin and troponin C", *Protein Engng.*, **4**, 625–637 (1991).

[12] J.-L. Pascual-Ahuir, E.L. Mehler and H. Weinstein, "Calmodulin structure and function: Implication of arginine residues in the compaction related to ligand binding", *Molec. Engng.*, **1**, 231–247 (1991).

[13] H. Weinstein and E.L. Mehler, "Structural specificity in the engineering of biological function: Insights from the dynamics of calmodulin", in *Molecular Aspects of Biotechnology: Computational Models and Theories*, (J. Bertran, Eds.) Kluwer Academic Publishers, Dordrecht, The Netherlands, 153–173 (1992).

[14] C. Gerday, L. Bolis and R. Gilles (Eds.), *Calcium and calcium binding proteins*; Springer-Verlag, Berlin (1988).

[15] A. Persechini, N.D. Moncrief and R.H. Kretsinger, "The EF-hand family of calcium-modulated proteins", *Trends in Neurosci.*, **12**, 462–467 (1989).

[16] C.A. McPhalen, N.C.J. Strynadka and M.N.G. James, "Calcium binding sites in proteins: A structural perspective", *Advan. Protein Chem.*, **42**, 77–144 (1991).

[17] N.C.J. Strynadka and M.N.G. James, "Towards an understanding of the effect of calcium on protein structure and function", *Current Opin. Struct. Biol.*, **1**, 905–914 (1991).

[18] M. Ikura, L.E. Kay, M. Krinks and A. Bax, "Triple-resonance multidimensional NMR study of calmodulin complexed with the binding domain of skeletal muscle myosin light-chain kinase: Indication of a conformational change in the central helix", *Biochemistry*, **30**, 5498–5504 (1991).

[19] W.E. Meador, A.R. Means and F.A. Quiocho, "Target enzyme recognition by calmodulin: 2.4 Å structure of a calmodulin-peptide complex", *Science*, **257**, 1251–1255 (1992).

[20] C.W. Heizmann (Eds.), *Novel Calcium-Binding Proteins*; Springer-Verlag, New York (1991).

[21] C.W. Heizmann and W. Hunziker, "Intracellular calcium-binding proteins: more sites than insights", *Trends in Biochem. Sci.*, **16**, 98–103 (1991).

[22] N.C.J. Strynadka and M.N.G. James, "Crystal structures of the helix-loop-helix calcium-binding proteins", *Ann. Rev. Biochem.*, **58**, 951–998 (1989).

[23] O. Herzberg and M.N.G. James, "Common structural framework of the two Ca2+/Mg2+ binding loops of troponin C and other Ca2+ binding proteins", *Biochemistry*, **24**, 5298–5302 (1985).

[24] F. Sussman and H. Weinstein, "On the ion selectivity in Ca-binding proteins: The cyclo(-L-Pro-Gly)3 peptide as a model", *Proc. Natl. Acad. Sci. USA*, **86**, 7880–7884 (1989).

[25] J.J. Falke, E.E. Snyder, K.C. Thatcher and C.S. Voertler, "Quantitating and engineering the ion specificity of an EF-hand-like Ca2+ binding site", *Biochemistry*, **30**, 8690–8697 (1991).

[26] O.D. Monera, G.S. Shaw, B.-Y. Zhu, B.D. Sykes, C.M. Kay and R.S. Hodges, "Role of interchain alpha-helical hydrophobic interactions in Ca2+ affinity, formation, and stability of a two-site domain in troponin C", *Protein Sci.*, **1**, 945–955 (1992).

[27] A. Persechini and R.H. Kretsinger, "Towards a model of the calmodulin-myosin light chain kinase complex: Implications for calmodulin function", *J. Cardiovasc. Pharm.*, **12(Suppl. 5)**, S1–S12 (1988).

[28] P.B. Heidorn, P.A. Seeger, S.E. Rokop, D.K. Blumenthal, A.R. Means, H. Crespi and J. Trewhella, "Changes in the structure of calmodulin induced by a peptide based on the calmodulin-binding domain of myosin light chain kinase", *Biochemistry*, **28**, 6757–6764 (1989).

[29] K.T. O'Neil and W.F. DeGrado, "How calmodulin binds its targets: sequence independent recognition of amphiphilic alpha-helices", *Trends Biochem. Sci*, **15**, 59–64 (1990).

[30] M. Kataoka, J.F. Head, T. Vorherr, J. Krebs and E. Carafoli, "Small-angl X-ray scattering study of calmodulin bound to two peptides corresponding to parts of the calmodulin-binding domain of the plasma membrane Ca2+ pump", *Biochemistry*, **30**, 6247–6251 (1991).

[31] N. Matsushima, Y. Izumi, T. Matsuo, H. Yoshino, T. Ueki and Y. Miyake, "Binding of both Ca^{2+} and mastoparan to calmodulin induces a large change in tertiary structure", *J. Biochem.*, **105**, 883–887 (1989).
[32] E.L. Mehler and H. Weinstein, "Computer – simulation studies of calmodulin and troponin C in solution", *Experientia*, **46**, A4 (1990).
[33] J.L. Pascual-Ahuir Weinstein, H., "The bending of calmodulin maybe modulated by its target protein", *Biophys. J.*, **59**, 118a (1991).
[34] D.M.E. Szebenyi and K. Moffat, "The refined structure of vitamin D-dependent calcium-binding protein from bovine intestine", *J. Biol. Chem.*, **261**, 8761–8777 (1986).
[35] Y.S. Babu, C.E. Bugg and W.J. Cook, "Structure of calmodulin refined at 2.2 A resolution", *J. Mol. Biol.*, **204**, 191–204 (1988).
[36] K.A. Satyshur, S.T. Rao, D. Pyzalska, W. Drendel, M. Greaser and M. Sundaralingam, "Refined structure of chicken skeletal muscle troponin C in the two-calcium state at 2-A resolution", *J. Biol. Chem.*, **263**, 1628–1647 (1988).
[37] O. Herzberg and M.N.G. James, "Refined crystal structure of Troponin C from turkey skeletal muscle at 2.0A resolution", *J. Mol. Biol.*, **203**, 761–779 (1988).
[38] R.H. Kretsinger, "Structure and evolution of calcium-modulated proteins", *CRC. Crit. Rev. Biochem.*, **8**, 118–174 (1982).
[39] R.H. Kretsinger, "Calcium-binding proteins", *Ann. Rev. Biochem.*, **45**, 239–262 (1976).
[40] S. Nakayama, N.D. Moncrief and R.H. Kretsinger, "Evolution of EF-hand calcium-modulated proteins. II. Domains of several subfamilies have diverse evolutionary histories", *J. Mol. Evol.*, **34**, 416–448 (1992).
[41] G. Barbato, M. Ikura, L.E. Kay, R.W. Pastor and A. Bax, "Backbone dynamics of calmodulin studied by 15N relaxation using inverse detected two-dimensional NMR spectroscopy: The central helix is flexible", *Biochemistry*, **31**, 5269–5278 (1992).
[42] R.E. Klevit, D.K. Blumenthal, D.E. Wemmer and E.G. Krebs, "Interaction of calmodulin and a calmodulin – binding peptide from myosin light chain kinase: Major spectral changes in both occur as the result of complex formation", *Biochemistry*, **24**, 8152–8157 (1985).
[43] R.E. Klevit, "Study of calmodulin – peptide interactions by NMR spectroscopy", *Methods Enzymol.*, **139**, 197–206 (1987).
[44] M. Kataoka, J.F. Head, B.A. Seaton and D.M. Engelman, "Melittin binding causes a large calcium-dependent conformational change in calmodulin", *Proc. Natl. Acad. Sci. USA*, **86**, 6944–6948 (1989).
[45] S. Linse, P. Brodin, T. Drakenberg, E. Thulin, P. Sellers, K. Elmden, T. Grundstrom and S. Forsen, "Structure-function relationships in EF-hand Ca2+-binding proteins. Protein engineering and biophysical studies of calbindin D9k", *Biochemistry*, **26**, 6723–6735 (1987).
[46] S. Linse, P. Brodin, C. Johansson, E. Thulin, T. Grundstrom and S. Forsen, "The role of protein surface charges in ion binding", *Nature*, **335**, 651–652 (1988).
[47] W.J. Chazin, J. Kordel, T. Drakenberg, E. Thulin, P. Brodin, T. Grundstrom and S. Forsen, "Proline isomerism leads to multiple folded conformations of calbindin D9k: Direct evidence from two-dimentional 1H NMR spectroscopy", *Proc. Natl. Acad. Sci. USA*, **86**, 2195–2198 (1989).
[48] S. Forsen, S. Linse, E. Thulin, B. Lindegard, S.R. Martin, P.M. Bayley, P. Brodin and T. Grundstrom, "Kinetics of calcium binding to calbindin mutants", *Eur. J. Biochem.*, **177**, 47–52 (1988).
[49] B. Svensson, B. Joensson and C. Woodward, "Electrostatic contribution to the binding of Ca2+ in calbinding mutants", *Biophys. Chem.*, **38**, 179–183 (1990).
[50] S. Linse, O. Teleman and T. Drakenberg, "Ca2+ binding to calbindin D9k strongly affects backbone dynamics: Measurements of exchange rates of individual amide protons using 1H NMR", *Biochemistry*, **29**, 5925–5934 (1990).
[51] M. Akke, S. Forsen and W.J. Chazin, "Molecular basis for co-operativity in Ca2+ binding to calbindin D9k", *J. Mol. Biol.*, **229**, 173–189 (1991).
[52] N.J. Skelton Kordel, J., Forsen, S., Chazin, W.J., "Comparative structural analysis of the calcium free and bound states of the calcium regulatory protein calbindin D9k", *J. Mol. Biol.*, **213**, 593–598 (1990).
[53] N.J. Skelton, J. Kordel, M. Akke and W.J. Chazin, "Nuclear magnetic resonance studies of the internal dynamics in apo, (Cd2+)1 and (Ca2+)2 calbindin D9k", *J. Mol. Biol.*, **227**, 1100–1117 (1992).
[54] D.B. Heidorn and J. Trewhella, "Comparison of the crystal and solution structures of calmodulin and troponin C", *Biochemistry*, **27**, 909–915 (1988).

[55] M. Akke, T. Drakenberg and W.J. Chazin, "Three-dimensional solution structure of Ca2+-loaded porcine calbindin D9k determined by NMR spectroscopy", *Biochemistry*, **31**, 1011-1020 (1992).

[56] F.C. Bernstein, T.F. Koetzle, G.J.B. Williams, E.F. Meyer, B.M.D., J.R. Rogers, D. Kennard, T. Simanouchi and M. Tatsumi, "The Protein Data Bank: A computer-based archival file for macromolecular structure", *J. Mol. Biol.*, **112**, 535-542 (1977).

[57] B.R. Brooks, R.E. Bruccoleri, B.D. Olafson, D.J. States, S. Swaminathan and M. Karplus, "CHARMM: A program for macromolecular energy, minimization and dynamics calculations", *J. Comput. Chem.*, **4**, 187-217 (1983).

[58] M.N. Liebman, C.A. Venanzi and H. Weinstein, "Structural analysis of carboxypeptidase A and its complexes with inhibitors as a basis for modeling enzyme recognition and specificity", *Biopolymers*, **24**, 1721-1758 (1985).

[59] J. Kordel, S. Forsen, T. Drakenberg and W.J. Chazin, "The rate and structural consequences of proline cis-trans isomerization in calbindin D9k: NMR studies of the minor (cis-Pro43) isoform and the Pro43Gly mutant", *Biochemistry*, **29**, 4400-4409 (1990).

[60] M. Billeter, "Comparison of protein structures determined by NMR in solution and by X-ray diffraction in single crystals", *Quart. Rev. Bioshys.*, **25**, 325-377 (1992).

[61] P. Ahlstrom, O. Teleman, J. Kordell, S. Forsen and B. Jonsson, "A molecular dynamics simulation of bovine calbindin D9k. Molecular structure and dynamics", *Biochemistry*, **28**, 3205-3211 (1989).

[62] K. Hori, J.N. Kushick and H. Weinstein, "Structural and energetic parameters of Ca2+ binding to peptides and proteins", *Biopolymers*, **27**, 1865-1886 (1988).

[63] E.L. Mehler and T. Solmajer, "Electrostatic effects in proteins: Comparison of dielectric and charge models", *Protein Engng.*, **4**, 903-910 (1991).

[64] E.L. Mehler and G. Eichele, "Electrostatic effects in water-accessible regions of proteins", *Biochemistry*, **23**, 3887-3891 (1984).

[65] M. Karplus and J.N. Kushick, "Methods for estimating the configurational entropy of macromolecules", *Macromolecules*, **14**, 325-332 (1981).

[66] S. Linse, C. Johansson, P. Brodin, T. Grundstrom, T. Drakenberg and S. Forsen, "Electrostatic contributions to the binding of Ca2+ in calbindin D9k", *Biochemistry*, **30**, 154-162 (1991).

[67] M. Levitt and R. Sharon, "Accurate simulation of protein dynamics in solution", *Proc. Natl. Acad. Sci. USA.*, **85**, 7557-7561 (1988).